Engineering Transactions, **74**(2): 327–354, 2026, https://doi.org/10.24423/engtrans.2025.3681
Institute of Fundamental Technological Research Polish Academy of Sciences (IPPT PAN)
Université de Lorraine • Poznan University of Technology

Technical Note

Analytical Approach and Shooting Method for the Solution of a Nonlocal Eringen Elasticity Problem of Nanorods

Aleksandra Manecka-Padaż[1)*], Ewa Eliza Rożko[1),2)], Zdzisław Nowak[1)], Piotr Chudziński[1)]

[1)] *Institute of Fundamental Technological Research, Polish Academy of Sciences*
Warsaw, Poland

[2)] *Institute of Outcomes Research, Maria Sklodowska-Curie Medical Academy*
Warsaw, Poland

[*]Corresponding Author: amanecka@ippt.pan.pl

The aim of this paper is to study the post-buckling behavior of nanorods, taking into account small scale effects. In this paper, the buckling of a nanorod column subjected to a tip load is investigated. The nanorod is on a clamped support at one end, while the other end is simply supported and subjected to axial compression. At this end, the nanorod is movable only in the horizontal direction. The governing differential equation describing the behavior of the nanorod is derived from the moment–curvature relationship, in analogy with the classical Euler–Bernoulli beam theory, together with the equilibrium equations, including the effects of nonlocal elasticity, as well as the corresponding boundary conditions. A numerical shooting method is derived and employed to solve the differential equations in this problem. The results, including nonlocal elasticity, reveal that nanorods have decreased structural stiffness and show a significant effect of geometrical parameters on the stability of buckled nanorods, emphasizing the importance of accounting for their interaction in the design of nanostructural systems.

Keywords: nonlocal elasticity theory, nanorods, small-scale effect, postbuckling behavior.

1. Introduction

For a slender elastic beam under axial compression, the classical Euler theory predicts a bifurcation of the straight configuration of the beam when the critical load is reached. The elastica problem was experimentally investigated by Pieter van Musschenbrock, see [1], and then mathematically studied by Bernoulli and Euler, see [2]. Finally, it was solved by Euler in 1744, who obtained nine classes of solutions of the elastic curve and named them elasticae, see [3]. Motivated by

recent progress in experiments on nanorods, here we study how these elastica solutions change upon adding nonlocality to the model, described by a single nonlocal parameter μ.

Over the years, many researchers have been interested in the elastica problem, and there exist many studies focused on various aspects of this issue. KIRCHHOFF [4] found an analogy between the equations describing the equilibrium state of an elastic rod and those describing the dynamics of a simple swinging pendulum. BORN [5] studied the exact elastica curves in his Ph.D. thesis. NISHINARI [6] partially analyzed the nonlinear dynamics of elastic rods and applied the soliton approach to analyze the nonlinear deformation of real elastic rods, clarifying the physical meaning of the assumed velocities. CHUCHEEPSAKUL and MONPRAPUSSORN [7] studied a highly nonlinear problem of instability of a flexible elastic pipe transporting fluid. They based their analysis on the inextensible elastica theory of rods, and the solution was obtained by using elliptic integrals and the numerical shooting method. VASSILEV *et al.* [8] presented the fluid membrane equilibrium shape equation in the form of a generalization of Euler's elastica. KIBACH *et al.* [9] investigated the post-buckled free vibration problem of an elastica around one of its vibration modes. The main contribution of their work is the detection of nonlinear frequencies of the elastica, i.e., its different backbone curves, around one of its post-buckled configurations, without any assumptions on the order of magnitude of curvature, rotation, or response. The detected nonlinear frequency relationships provide tools for tuning parameters of the elastica in order to achieve specific types of behavior around one of its buckling and vibration modes.

In the paper by TALONI *et al.* [10], a general expression for the strain energy of a homogeneous, isotropic, plane extensible elastic body with an arbitrary undeformed configuration was derived. This expression appears to be suitable for one-dimensional models of polymers or vesicles, whose natural configuration is characterized by locally changing curvature. The authors discuss the relevance of their model for describing real biological non-homogeneous filaments. LEANZA *et al.* [11] determined the axial buckling behavior for an elastic beam or rod with uniform natural curvature. In the elastica problems, this significantly enriches the variety of buckling behaviors exhibited by rods or beams that are straightened by pure bending and clamped at their ends. While the classical elastica displays stable post-buckling behavior, the elastica with natural curvature exhibits a wide range of behaviors from stable to highly unstable. The stability of the interesting limiting case, in which the maximum uniform natural curvature is imposed on a rod or beam clamped at both ends, has also been determined via initial post-bifurcation analysis.

PHUNGPAINGAM and CHUCHEEPSAKUL [12] analyzed the behavior of a variable-arc-length elastica subjected to end loading with a rotational spring

joint within the span length of the elastica. Lai *et al.* [13] investigated the buckling behavior of the compression of high-strength concrete-encased steel columns through experimental, numerical and analytical analyses. Wang *et al.* [14] studied the instability of an elastica under bilateral displacement control at a material point. Fraldi *et al.* [15] studied both compressive and tensile buckling in the case of human finger luxation, demonstrating that the phenomenon can be interpreted as an elastic bifurcation in a natural system. Hathaipichitchai *et al.* [16] investigated the post-buckling behavior of a variable-arc-length elastica pipe caused by internal fluid transport motion, including the effect of pressure variability. Curatolo *et al.* [17] employed a modified Euler elastica model for optimizing catapult mechanism conditions due to the catapult emerging in a soft rod. Wang and Qiu [18] proposed an extended elastica-plastica theory for Euler–Bernoulli beams. Matsutani [19] studied the mechanics of elastica as a model for the shapes of supercoiled DNA. The elastica problem has been intensively investigated over the years and has played a major role in the development of mathematics, including Jacobi elliptic functions and also numerical methods.

In recent decades, nanotechnology has been a main subject of interest for researchers from all over the world. Materials such as thin films, nanorods, and nanotubes may exhibit unusual properties not noticed at the macroscale [20]. Modeling and optimization of nanoscale devices require an extended characterization of material at such a small scale. The elastica issue at the nanoscale has also become of great interest over time. Wang and Feng [21] measured the mechanical properties of compressed nanowires based on the Euler buckling model. Moradi *et al.* [22] examined the mechanical behavior of polystyrene nanorods using the classical Euler–Bernoulli beam model.

Recently, further studies at the nanoscale have been undertaken, mainly based on Eringen's nonlocal elasticity theory. This theory assumes that the stress at a point is a function of the strains at adjacent points in the continuum [23]. This approach has become an efficient tool for the analysis of the influence of size effects in small-scale structures. Thongyothee and Chucheepsakul [24] investigated the stability of nanobeams, including small-scale effects and surface stress. Challamel *et al.* [25] studied the elastica problem using an equivalent nonlocal continuum approach and compared it with a discrete physical model. Lembo [26] researched post-buckling configurations of nanorods with various end conditions using Eringen's nonlocal theory. A comparison of results for nonlocal and classical rods showed a significant impact of the nonlocal parameter on the post-buckling behavior of rods.

Tang and Qing [27] numerically examined the effects of nonlocal parameters on static bending, elastic buckling, and free vibration of Timoshenko beams under different boundary and loading conditions. Their study showed

that a consistent softening effect can be obtained. Hussain and Naeem [28] applied Eringen's theory to calculate the frequency of single-wall carbon nanotubes (SWCNT). The outcome revealed that increasing the nonlocal parameter results in significantly reducing the natural frequencies of the SWCNT. Berecki *et al.* [29] compared Eringen's two-phase local/nonlocal model with Eringen's differential model in order to perform bifurcation analysis of a nanotube through which a nanostring passes.

It is also worth mentioning that an interesting result was obtained using the integral (stress-driven) form of nonlocal elasticity theory. Darban *et al.* [30] investigated size-dependent buckling of cracked nanocantilevers, with results applicable to a wide range of mechanical nanosensors. In [31], Darban analyzed nonuniform beams with multiple sub-beams. The model was based on a stress-driven nonlocal theory, which can be applied to control the flexural response of a nanobeam. In [32], Darban's approach provides explicit solutions for displacements and deflections, showing how size effects alter beam stiffness and behavior relative to classical theory using a variational approach and a transfer matrix method.

Although Eringen's nonlocal theory provides valuable analytical frameworks, most practical problems – especially those involving complex boundary conditions or nonlinear constitutive terms – require robust numerical techniques for their solution. Several computational methods have therefore been developed and applied within the nonlocal elasticity framework. The finite difference method (FDM) and the finite element method (FEM) remain the most frequently used numerical tools for static and dynamic analyses of nonlocal beams and plates, as reported by Reddy *et al.* [33], Phadikar and Pradhan [34]. The differential quadrature method (DQM) has also been implemented successfully for solving higher-order nonlocal governing equations, providing excellent accuracy for small-scale effects [35].

In addition, variational and Galerkin formulations were proposed by Challamel and Wang [36] to handle mixed local–nonlocal boundary conditions and to study bifurcation phenomena. For nonlinear problems, especially in buckling and post-buckling regimes, the shooting method has proven to be a reliable approach, offering high numerical stability and physical interpretability [37, 38]. Recently, a stress-driven nonlocal theory based on the Bernoulli–Euler model was presented for size-dependent free vibrations of nanobeams with multiple edge cracks [39].

These numerical developments confirm that, while the classical analytical formulations of the nonlocal theory remain essential for model validation, the integration of advanced computational techniques is crucial for studying complex geometries, heterogeneity, and boundary interactions in nanostructures. The numerical solution of Eringen's nonlocal beam equation requires a robust and ac-

curate method capable of handling nonlinear second-order boundary value problems (BVPs) with boundary conditions prescribed at opposite ends of the spatial domain. As demonstrated in several recent works (e.g., [40]), classical numerical approaches such as FDM or collocation schemes often fail when applied to highly nonlinear systems, especially those involving nonlocal constitutive terms. In the case of Eringen's beam, the governing equation contains nonlinear denominators of the form $(EI - \mu F\cos(\theta(s))) - 1(EI - \mu F\cos\theta(s)) - 1$, which can lead to local singularities and numerical instabilities when using grid-based methods.

As shown, there are plenty of works that focus on the elastica problem. Elastica theory plays an important role in the study of large displacements of slender rods. However, the majority of these studies are still limited to purely elastic material. In [41], the traditional elastica theory was extended to an elastica-plastica theory. However, buckling analysis remains not fully understood, especially at the nanoscale. This paper is, therefore, devoted to studying the influence of nonlocal theory on the post-buckling behavior of nanorods. The validity of the method proposed in this paper is confirmed through comparison with existing researches. The current results are expected to be useful for predicting nanorod strength and for the design of nanostructures and nanodevices related to nanorods.

The paper is divided into five sections. In Sec. 2, we formulate the elastica problem in the presence of nonlocal strain in the form of a second-order ordinary differential equation. We also discuss the value of the critical load causing the loss of structural stability. Section 3 presents our numerical solution using the built-in shooting method in *Wolfram Mathematica*, combining adaptive Runge–Kutta integration with iterative boundary-condition correction. In Sec. 4, we report the results and analyze the influence of the nonlocal parameter. Section 5 provides concluding remarks. In Appendix, an analytical solution for the local nonlinear elasticity theory is provided.

2. Elastica problem

First, in order to study scale effect in the elastica problem, Eringen's nonlocal theory is applied. Then, a numerical study of this problem is shown. Moreover, the critical load value calculations are demonstrated.

2.1. Nonlocal theory formulation

The nonlocal stress-gradient theory combines aspects of both nonlocal elasticity and stress-gradient theories, thereby considering both long-range interactions and higher-order stress gradients. Within this framework, the stress state

at a point x is influenced by the strains at all other points in the body. In particular, the nonlocal stress-gradient theory can be reduced to both classical nonlocal elasticity theory and stress-gradient theory, hence offering a comprehensive method that encompasses both theoretical concepts. The nonlocal elasticity theory was initially formulated by ERINGEN [42] and ERINGEN and EDELEN [43] by means of an integral constitutive equation. Within the framework of continuum mechanics, the nonlocal elasticity theory proposed by Eringen has become a widely used approach for modeling structures at the nanoscale.

The only nonzero strain in the Euler–Bernoulli beam theory, accounting for the Kirchhoff assumption, is [24]:

$$\varepsilon_{xx} = \frac{\mathrm{d}u_1}{\mathrm{d}x} - y\frac{\mathrm{d}^2 u_2}{\mathrm{d}x^2} = \varepsilon_{xx0} + y\kappa, \tag{2.1a}$$

where $\varepsilon_{xx0} = \frac{\mathrm{d}u_1}{\mathrm{d}x}$ is the extensional strain and $y\kappa$ represents the bending strain.

Eringen's theory can be expressed either in an integral form, which explicitly accounts for long-range interactions, or in an equivalent differential form that is often more convenient for analytical and numerical treatment. In this paper, Eringen's differential form is examined, and the governing equations for the nonlocal model can be written as [44]:

$$\sigma_{xx} - \mu\frac{\mathrm{d}^2\sigma_{xx}}{\mathrm{d}x^2} = E\varepsilon_{xx}, \tag{2.1}$$

where σ_{xx}, ε_{xx}, E, and μ denote the normal stress, normal strain, Young's modulus, and the nonlocal parameter, respectively. The model of an elastic medium based on the equation of state (2.1), and its relationship with Eringen's nonlocal theory, was also analyzed by ROMANO and BARRETTA [45], and by other researchers, e.g., NOBILI and PRAMANIK [46]. BARRETTA *et al.* [47] identified a simple constitutive strategy for nanotechnological applications using an improved differential law with contributions from FERNÁNDEZ-SÁEZ *et al.* [48]. The newly developed method is consistent with the integral method [47]. The present work is motivated by the enhanced Eringen's differential model for all boundary conditions developed by BARRETTA *et al.* [47]. It has to be emphasized, however, that the connection between the differential and integral forms is still an open question. The equations are based on a specific assumption about the propagator (kernel) in the integral form. Several recent works have investigated various forms of propagators and the constitutive boundary conditions they imply, see, e.g., [49–58].

Both approaches – integral and differential – require the use of material and geometric parameters, and their clear interpretation is necessary for accurate analysis. The effect of nonlocality is incorporated into the constitutive differential Eq. (2.1) by the nonlocal parameter μ. The nonlocal parameter value

TABLE 1. Various ways to introduce the nonlocal parameter.

Parameter	Symbol	Magnitude	Researcher	Material
Internal characteristic length [nm]	a	0.142	ERINGEN [44]	Carbon nanostructures
Scale coefficient	e_0	0.39; 0.50; 0.70	TIMESLI [61]	Mathematical model
		0.288–0.5	WANG, ZHANG [62]	Carbon nanostructures
		0–1	REDDY, PANG [63]	Carbon nanotubes
		0.288	WANG, HU [64]	Carbon nanostructures
		0.39	ERINGEN [44]	Single-walled carbon nanotubes
Product of nonlocal parameter and internal characteristic length [nm]	e_0a	1	AKPINAR *et al.* [65]	Carbon nanorods and nanotubes
		0; 2.0; 4.0	NATSUKI *et al.* [66]	Single-walled carbon nanotubes
		1	UZUN *et al.* [67]	Porous functionally graded nanostructures
		0; 1.0; 1.5	EBRAHIMI [68]	Single-walled carbon nanotubes
		0.5	MURMU [69]	Single-walled carbon nanotubes
		0–1	WANG *et al.* [70]	Single-walled carbon nanotubes
Nonlocal parameter squared	$\mu = (e_0a/l)^2$	0-1	KHANIKI [71]	Carbon nanorod
		0.04	THONGYOTHEE [72]	Mathematical model
Nonlocal parameter	e_0a/h_0	0–0.8	KARLIČIĆ, MURMU [59]	Multi-walled carbon nanotubes
		0–0.6	LU [73]	Multi-walled carbon nanotubes
Normalized nonlocal parameter	$\psi = e_0a/l$	0–0.20	DE ROSA *et al.* [74]	Single-walled carbon nanotubes

depends on the material and the geometry of the element and it is largely determined experimentally; however, the exact value of the nonlocal parameter μ is still not known. Here, we take it as a free parameter in order to study its influence. Table 1 provides a literature overview of the main terms used for the nonlocal theory description; here, e_0 denotes a material constant, a is an internal characteristic length, which can represent a granular size or the distance between C-C bonds [59], and e_0 is a characteristic magnitude of the structure, for example, the nanotube diameter [60].

Table 1 summarizes different ways in which researchers have introduced the nonlocal parameter in Eringen's nonlocal elasticity theory, highlighting the lack of a single universal definition. The reported values vary depending on the adopted model, material characteristics, and the methodological choices. Importantly, research in this field is still very active, and new studies continue to refine the interpretation and application of the nonlocal parameter to improve predictive models for advanced nanomaterials. In this study, we aim to evaluate the nonlocal parameter value to contribute to the ongoing discussion, provide further insights into its proper application, and establish hypotheses for subsequent experimental validation.

The standard theory for describing the buckling phenomenon is the well-established Euler theory. This is the starting point of our calculations, and we present it in Appendix. In Euler's theory, we describe the deflection and change in the curvature of the compressed rod due to the applied force. Equation (A.7) and Eq. (A.8) can be used to plot elastics to calculate the deflection and displacement of the rod's end. In this work, we use Eringen's theory to describe the deflected shape of the nanorods, where the moment-curvature equation (Eq. (A.3)) is modified into [44]:

$$\frac{\mathrm{d}\theta(s)}{\mathrm{d}s} = -\frac{1}{EI}\left(M - \mu\frac{\mathrm{d}^2 M}{\mathrm{d}x^2}\right), \tag{2.2}$$

where M is the bending moment at any point along the rod axis, and the nonlocal part is expressed by the second derivative of the moment.

The study introduces a differential version of Eringen's nonlocal beam theory for elastic materials, constructed separately from the original integral framework. Our aim now is to solve Eq. (2.2) and obtain a solution that can estimate the influence of the nonlocal parameter μ on the elastica shape.

The small segment shown in Fig. 1 is consistent with the calculations presented further and is provided for discussion. In this work, we adopt a reference frame that is more suitable for our purposes; however, we wish to emphasize that it is the reverse of the one used in [24], due to adaptation to the coordinate system applied here.

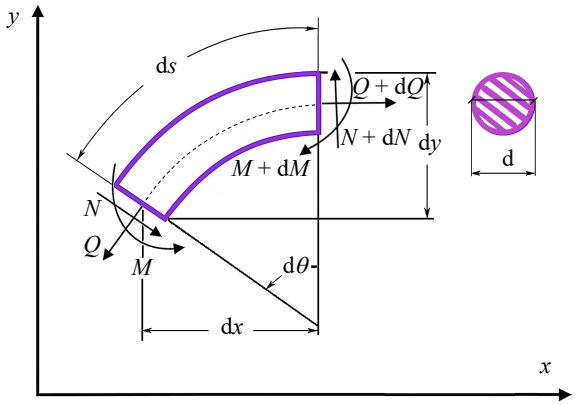

FIG. 1. Small segment of the compressed nanorod shown in the present reference frame (based on [24]).

The equilibrium equations relating the gradients of the normal force N, shear force Q, and bending moment M along the arc-length s to the curvature κ are as follows:

$$\frac{\mathrm{d}N}{\mathrm{d}s} = \kappa Q, \tag{2.3}$$

$$\frac{\mathrm{d}Q}{\mathrm{d}s} = -\kappa N, \tag{2.4}$$

$$\frac{\mathrm{d}M}{\mathrm{d}s} = Q. \tag{2.5}$$

Then, in Eringen's notation:

$$\frac{\mathrm{d}M}{\mathrm{d}x} = \frac{\mathrm{d}M}{\mathrm{d}s} \cdot \frac{\mathrm{d}s}{\mathrm{d}x} = \eta Q. \tag{2.6}$$

The factor $\frac{\mathrm{d}s}{\mathrm{d}x}$ is not defined; however, it is established that strain may be expressed in this form, namely:

$$\sigma_{(\mathrm{d}s)} = E\varepsilon_{(\mathrm{d}s)}, \tag{2.7}$$

where E, $\sigma_{(\mathrm{d}s)}$, and $\varepsilon_{(\mathrm{d}s)}$ denote Young's modulus, normal stress, and strain, respectively.

The normal strain can be measured as the difference between the current and reference configurations along the axis, and the unknown factor $\frac{\mathrm{d}s}{\mathrm{d}x}$ can be denoted as η:

$$\varepsilon_{(\mathrm{d}s)} = \frac{\mathrm{d}s}{\mathrm{d}x} - \frac{\mathrm{d}x}{\mathrm{d}x} = \eta - 1. \tag{2.8}$$

As is well known, the stress $\sigma_{(ds)}$ can be expressed in terms of the axial normal force N and the cross-sectional area A as:

$$\sigma_{(\mathrm{d}s)} = \frac{N}{A}. \tag{2.9}$$

We can now express Eq. (2.7) as follows:

$$\frac{N}{A} = E\,(\eta - 1)\,, \tag{2.10}$$

$$\eta = \frac{N}{EA} + 1. \tag{2.11}$$

The bending behavior is described by the bending moment M. As it is presented in Fig. 2 for the loading considered, this moment is caused by the axial force F acting at the deflection $u_2(s)$:

$$M = Fu_2(s). \tag{2.12}$$

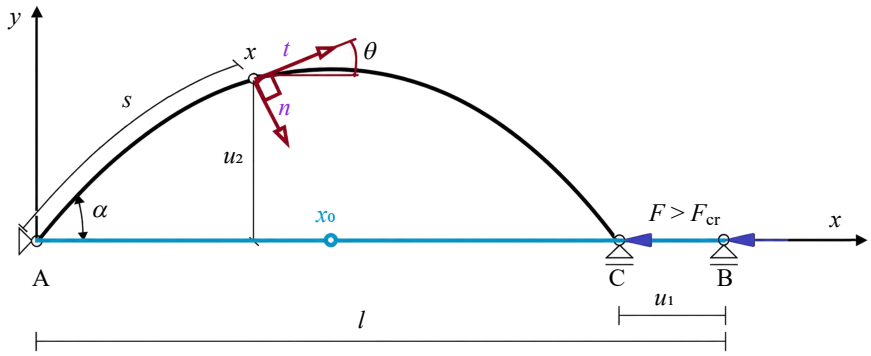

FIG. 2. Compression of the rod due to the applied force F.

The corresponding shear force Q is obtained as the derivative of the bending moment with respect to the arc-length coordinate s. Making use of the kinematic relation between deflection and rotation angle of the cross-section $\theta(s)$ leads to:

$$Q = \frac{\mathrm{d}M}{\mathrm{d}s} = \mathrm{d}\frac{Fu_2(s)}{\mathrm{d}s} = F\sin\theta(s). \tag{2.13}$$

We can now express Eq. (2.3) as follows:

$$N = \frac{-1}{\frac{\mathrm{d}\theta(s)}{\mathrm{d}s}} \cdot \frac{\mathrm{d}Q}{\mathrm{d}s} = \frac{-1}{\frac{\mathrm{d}\theta(s)}{\mathrm{d}s}} \cdot \frac{\mathrm{d}}{\mathrm{d}s}\left(F\sin\theta(s)\right) \tag{2.14}$$

$$= \frac{-1}{\frac{\mathrm{d}\theta(s)}{\mathrm{d}s}} \cdot F\cos\theta(s)\frac{\mathrm{d}\theta(s)}{\mathrm{d}s} = -F\cos\theta(s).$$

We can express η as

$$\eta = \frac{N}{EA} + 1 = -\frac{F\cos\theta(s)}{EA} + 1. \tag{2.15}$$

Then:

$$\frac{\mathrm{d}M}{\mathrm{d}x} = \frac{\mathrm{d}M}{\mathrm{d}s} \cdot \frac{\mathrm{d}s}{\mathrm{d}x} = \eta Q = \left(\frac{N}{EA} + 1\right) \cdot Q. \tag{2.16}$$

Then, we can obtain:

$$\begin{aligned} \frac{\mathrm{d}^2M}{\mathrm{d}x^2} = \frac{\mathrm{d}}{\mathrm{d}x}\left(\frac{QN}{EA} + Q\right) &= \frac{1}{EA}\frac{\mathrm{d}}{\mathrm{d}x}(QN) + \frac{\mathrm{d}Q}{\mathrm{d}x} \\ &= \frac{1}{EA}\left(\frac{\mathrm{d}Q}{\mathrm{d}x} \cdot N + \frac{\mathrm{d}N}{\mathrm{d}x} \cdot Q\right) + \frac{\mathrm{d}Q}{\mathrm{d}x}. \end{aligned} \tag{2.17}$$

Subsequently, the derivatives are determined:

$$\frac{\mathrm{d}Q}{\mathrm{d}x} = \frac{\mathrm{d}Q}{\mathrm{d}s} \cdot \eta = -\kappa\eta N, \tag{2.18}$$

$$\frac{\mathrm{d}N}{\mathrm{d}x} = \frac{\mathrm{d}N}{\mathrm{d}x} \cdot \eta = \kappa\eta Q. \tag{2.19}$$

Then, using Eq. (2.18) and Eq. (2.19), we obtain:

$$\frac{\mathrm{d}^2M}{\mathrm{d}x^2} = \frac{1}{EA}\left(-\kappa\eta N^2 + \kappa\eta Q^2\right) - \kappa\eta N = \frac{1}{EA}\left(\kappa\eta\left(Q^2 - N^2\right)\right) - \kappa\eta N. \tag{2.20}$$

Then, using Eq. (2.2), we obtain:

$$\frac{\mathrm{d}\theta(s)}{\mathrm{d}s} = -\frac{1}{EI}\left(M - \mu\left(\frac{1}{EA}\left(\frac{\mathrm{d}\theta(s)}{\mathrm{d}s}\eta\left(Q^2 - N^2\right)\right) - \frac{\mathrm{d}\theta(s)}{\mathrm{d}s}\eta N\right)\right), \tag{2.21}$$

$$\frac{\mathrm{d}\theta(s)}{\mathrm{d}s}\left(1 - \frac{\mu}{EIEA}\eta\left(Q^2 - N^2\right) + \frac{\eta\mu N}{EI}\right) = -\frac{M}{EI}, \tag{2.22}$$

$$\frac{\mathrm{d}\theta(s)}{\mathrm{d}s} = -\frac{M}{EI} \cdot \left(\frac{1}{1 - \frac{\mu\eta}{EIEA}\left(Q^2 - N^2\right) + \frac{\eta\mu N}{EI}}\right). \tag{2.23}$$

This expression is identical to that given in [24].

Now, we seek the second derivative of θ with respect to s:

$$\frac{\mathrm{d}^2\theta}{\mathrm{d}s^2} = -\frac{1}{EI}\frac{\mathrm{d}}{\mathrm{d}s}\left(\frac{M}{1 - \frac{\mu\eta}{EIEA}\left(Q^2 - N^2\right) + \frac{\eta\mu N}{EI}}\right). \tag{2.24}$$

Expanded versions of Eq. (2.24) after substituting the physical quantities are as follows:

$$\frac{\mathrm{d}^2\theta}{\mathrm{d}s^2} = -\frac{1}{EI}\frac{\mathrm{d}}{\mathrm{d}s}\left(\frac{Fu_2(s)}{a^*}\right), \tag{2.25}$$

$$\frac{\mathrm{d}^2\theta}{\mathrm{d}s^2} = -\frac{1}{EI}\frac{\mathrm{d}}{\mathrm{d}s}\left(\frac{Fu_2(s)}{b^*}\right), \tag{2.26}$$

where

$$a^* = 1 - \frac{\mu}{EIEA}\left(F^2 - \frac{F^3\cos\theta(s)}{EA} + \frac{2F^3\cos^3\theta(s)}{EA} - 2F^2\cos^2\theta(s)\right) + \left(\frac{\mu F^2\cos^2\theta(s)}{EIEA} - \frac{\mu F\cos\theta(s)}{EI}\right),$$

$$b^* = 1 - \frac{\mu F^2}{EIEA} + \frac{\mu F^3\cos\theta(s)}{EIEAEA} - \frac{2\mu F^3\cos^3\theta(s)}{EIEAEA} + \frac{3\mu F^2\cos^2\theta(s)}{EIEA} - \frac{\mu F\cos\theta(s)}{EI}.$$

To the best of our knowledge, Eq. (2.26) with the second derivative has not been presented in the literature. It is worth mentioning that for $\mu = 0$, Eringen's theory reduces to the classical Euler's theory (see Eq. (A.2)).

2.2. Critical load value

According to Euler's theory, we can calculate the critical load causing the loss of the stability of the structure using the following formula [75]:

$$P_{crE} = EI\left(\frac{\pi n}{l}\right)^2, \tag{2.27}$$

where $n = 0, 1, 3...$

From the engineering point of view, it is very useful to apply this formula to obtain a discrete set of values of the load for a particular material to prevent buckling phenomena. However, in nonlinear elasticity theory, the critical load value is not a constant and depends on the elliptic integral of the first kind $K(k)$, related to the initial angle $\alpha = \theta(0)$. We can calculate it using Bigoni's formula [76]:

$$P_{cr} = EI\left(\frac{m}{l}\right)^2\left[2K\left(\sin\frac{\alpha}{2}\right)\right]^2. \tag{2.28}$$

Equation (2.28) is used in Sec. 3 in order to estimate the reference axial force value.

3. Numerical solution of the elastica problem

3.1. Method

In this section, we adopt the shooting method, as implemented in *Wolfram Mathematica*, to obtain the solution of the second-order nonlinear differential equation governing the nonlocal Eringen's beam (Eq. (2.26)). This approach converts a boundary value problem (BVP) into an equivalent initial value problem (IVP), which is iteratively solved until the boundary conditions at both ends of the beam are satisfied.

The shooting method was chosen because of its numerical stability and robustness when dealing with nonlinear differential equations containing trigonometric terms and variable coefficients in the denominator, such as in Eringen's model. Alternative approaches, such as finite difference or collocation methods, often lead to convergence issues near points where the denominator in Eq. (2.26) becomes small. In contrast, the shooting method allows direct control over the boundary conditions and provides stable convergence even for strongly nonlinear systems.

In the numerical implementation, the built-in solver *NDSolve* was used with the option: Method → 'Shooting'. This solver internally applies an adaptive Runge–Kutta algorithm of variable order (Dormand–Prince/Fehlberg type). The algorithm automatically adjusts both the integration step and the order according to the local truncation error, ensuring high accuracy while maintaining computational efficiency.

3.2. Implementation details

The final algorithm was implemented as a BVP, solved by the built-in shooting method in *Wolfram Mathematica*. The governing system consisted of three first-order differential equations:

$$\theta'(s) = \kappa(s), \tag{3.1}$$

$$\kappa'(s) = -\frac{F}{EI - \mu F \cos\theta(s)} \sin\theta(s), \tag{3.2}$$

$$u_2'(s) = \sin\theta(s), \tag{3.3}$$

with mixed Dirichlet–von Neumann (clamped–pinned) boundary conditions:

$$\theta(s = 0) = \alpha, \tag{3.4}$$

$$\theta'(s = l) = 0, \tag{3.5}$$

$$u_2'(s = l) = 0. \tag{3.6}$$

These boundary conditions are motivated by recent experiment on nanorods reported by MANECKA-PADAŻ *et al.* [77]. The algorithm treats the initial curvature $\kappa(0)$ as a shooting parameter. For an assumed value of $\kappa(0)$, the system is integrated from $s = 0$ to $s = l$ using an adaptive Runge–Kutta scheme (Dormand–Prince type [78, 79]). After each integration, two residuals are evaluated:

$$R_1 = \theta'(l; \kappa(0)), \tag{3.7}$$

$$R_2 = u_2'(l; \kappa(0)). \tag{3.8}$$

The initial slope $\kappa(0)$ is then iteratively corrected using a secant or Newton-type update until both residuals satisfy the prescribed tolerance ($|R_1|, |R_2| < 10^{-6}$).

This procedure ensures that the end of the beam satisfies both mechanical and geometric constraints simultaneously. The adaptive step-size control built into the solver prevents numerical instabilities near regions where $EI - \mu F \cos\theta(s)$ approaches zero, ensuring smooth convergence even for relatively large values of the nonlocal parameter μ. The critical value μ_{cr} decreases with increasing value of initial angle $\alpha = \theta(0)$. This hybrid approach combines the accuracy of adaptive integration with the flexibility of iterative boundary correction, offering excellent numerical stability and control of the solution error. Moreover, the adaptive step-size control allows the solver to handle regions with steep curvature gradients or strong geometric nonlinearity without loss of accuracy.

The choice of the shooting method is also justified from a physical standpoint. Unlike mesh-based numerical techniques, which require additional artificial constraints, the shooting method directly mirrors the physical process of 'matching' the beam shape to the boundary conditions. This makes it particularly suitable for bifurcation-type problems and for analyzing stability modes of nanobeams.

3.3. Model parameters and reference force

In the numerical simulations, the material and geometric parameters were chosen to represent a slender nanobeam of length $l = 1000\,\text{nm}$. The selected values correspond to realistic mechanical properties of nanostructures such as silicon nanobridges or carbon nanotubes and are consistent with earlier studies based on the Euler–Bernoulli beam model.

Numerical simulations were performed for a normalized beam model with the parameters $l = 1000\,\text{nm}$ and $EI = EA = 1$, $m = 1$, and $\mu \in \{0; 0.01; 0.02, 0.03; 0.04; 0.05\}$. The parameters EI and EA were selected to ensure compatibility with the local Euler–Bernoulli model in the limit $\mu \to 0$, allowing direct comparison between classical and nonlocal solutions. To provide a consistent basis for comparison between local and nonlocal models, the reference axial force F was defined according to Eq. (2.28) mentioned in Subsec. 2.2. Employing Euler's

critical force as the reference value ensures both physical and numerical consistency between the local and nonlocal formulations. This choice allows a direct evaluation of how the nonlocal parameter μ modifies the effective stiffness and the beam curvature distribution. As μ increases, the computed results reveal a clear structural softening effect: the deformation becomes more developed and the effective rigidity $EI_{\text{eff}} = EI - \mu F \cos\theta(s)$ decreases, confirming the expected nonlocal influence predicted by Eringen's theory.

The values of EI and EA for a circular cross-section (as in Fig. 1) can be calculated as

$$EI = \frac{E\pi \,\mathrm{d}^4}{64}, \tag{3.9}$$

$$EA = \frac{E\pi \,\mathrm{d}^2}{4}. \tag{3.10}$$

4. Results

The numerical results obtained with this method showed good agreement with the classical Euler–Bernoulli solutions for $\mu = 0$. For increasing values of the nonlocal parameter μ, a clear structural softening effect was observed. This effect manifests as a reduction in the effective stiffness and a smoother distribution of curvature along the beam length, confirming the expected influence of nonlocality within Eringen's framework. The resulting solutions $\theta(s)$ and $u_2'(s)$ were subsequently used to reconstruct the beam profile $y(x)$.

In Fig. 3, we see that as the nonlocal parameter μ increases, the angle θ increases along the curvilinear coordinate s. For equal increments in μ, this change becomes more pronounced at higher values – there is a smaller difference in θ between $\mu = 0.01$ and $\mu = 0.03$ than between $\mu = 0.03$ and $\mu = 0.05$. With increasing initial angle $\alpha = \theta(0)$, this effect becomes less evident, and the θ-profile becomes more slender. For larger α (i.e., $\alpha = 95^\circ$ and 118°), the trend reverses: a critical point appears (the larger the α, the earlier it occurs), beyond which θ falls below the prediction of the local theory as s varies. In the θ' plot, the influence of μ on the rod curvature is substantial and it intensifies with increasing initial angle α. Further quantitative analysis of the results shown in Fig. 3 is presented in Table 2. To satisfy the boundary conditions, it was necessary to assume an extension of the nanorod, denoted as δl. For each μ, the necessary change in beam length δl is reported. We see that δl increases with μ and is largest for the smallest initial angles α.

As it is presented in Fig. 4, the shape of the elastica $y(x)$ also changes noticeably under the nonlocal theory. A softening of the compressed rod is evident – the larger the nonlocal parameter μ, the more compliant the rod becomes to shape change. The curves obtained under the nonlocal theory resemble those

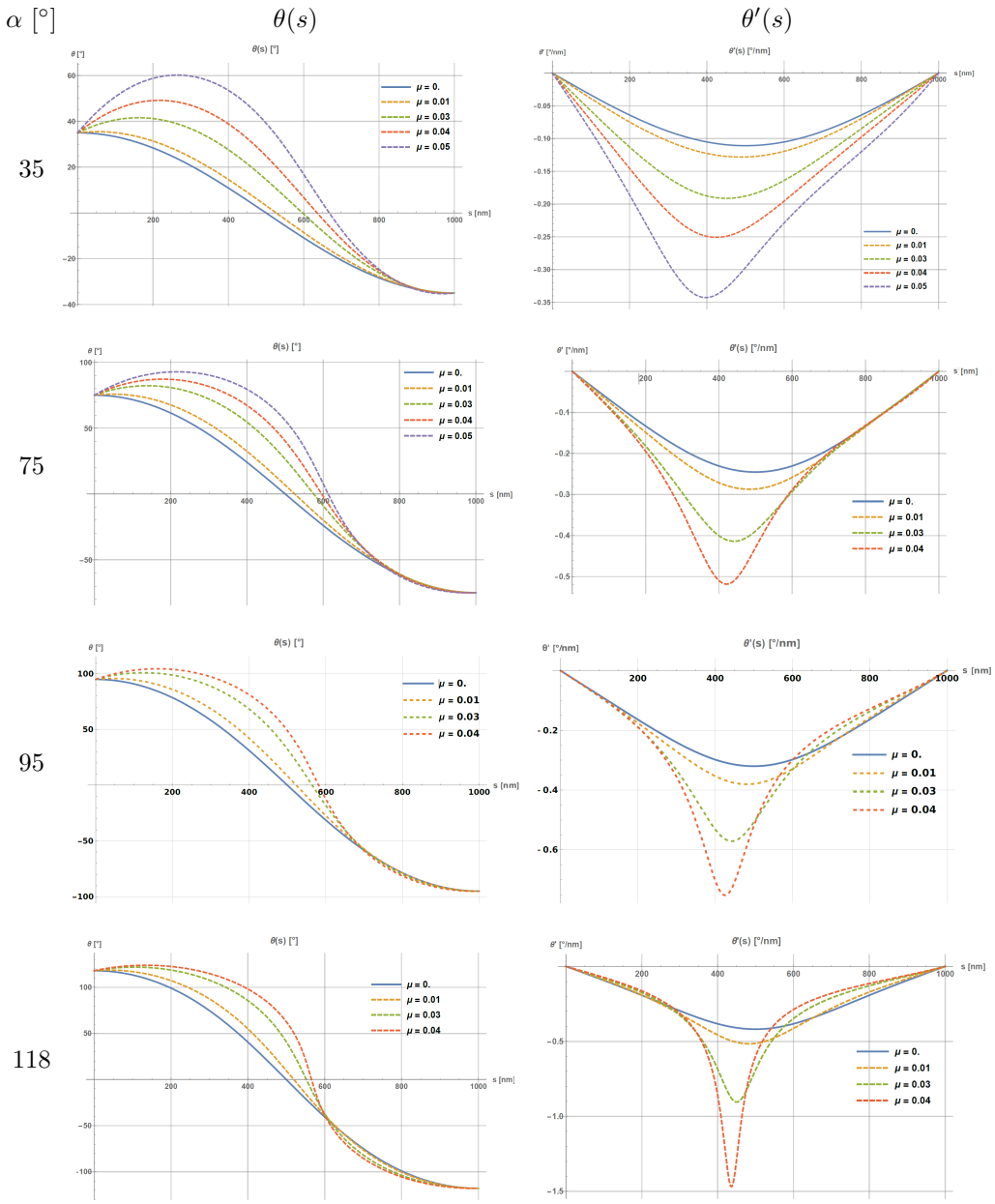

FIG. 3. Set of bending angles θ and their derivatives as functions of the curvilinear coordinate s. We present four pairs of plots for four different initial angles $\alpha = \theta(0)$. In each panel, results for different values of nonlocal parameters μ are shown.

corresponding to higher angles in the local theory (e.g., for $\alpha = 95°$, disregarding the boundary condition, the deformation pattern is similar to that of the local theory for 120°).

TABLE 2. Quantitative analysis of the results shown in Fig. 3.

μ	$\alpha = 35°$		$\alpha = 75°$		$\alpha = 95°$		$\alpha = 118°$	
	Δl [nm]	$\Delta l/l$ [%]	Δl [nm]	$\Delta l/l$ [%]	Δl [nm]	$\Delta l/l$ [%]	Δl [nm]	$\Delta l/l$ [%]
0.01	49.71	4.97	46.80	4.68	43.85	4.39	37.87	3.79
0.03	144.64	14.46	128.81	12.88	118.45	11.85	101.40	10.14
0.04	183.35	18.34	163.45	16.35	150.79	15.08	129.75	12.98

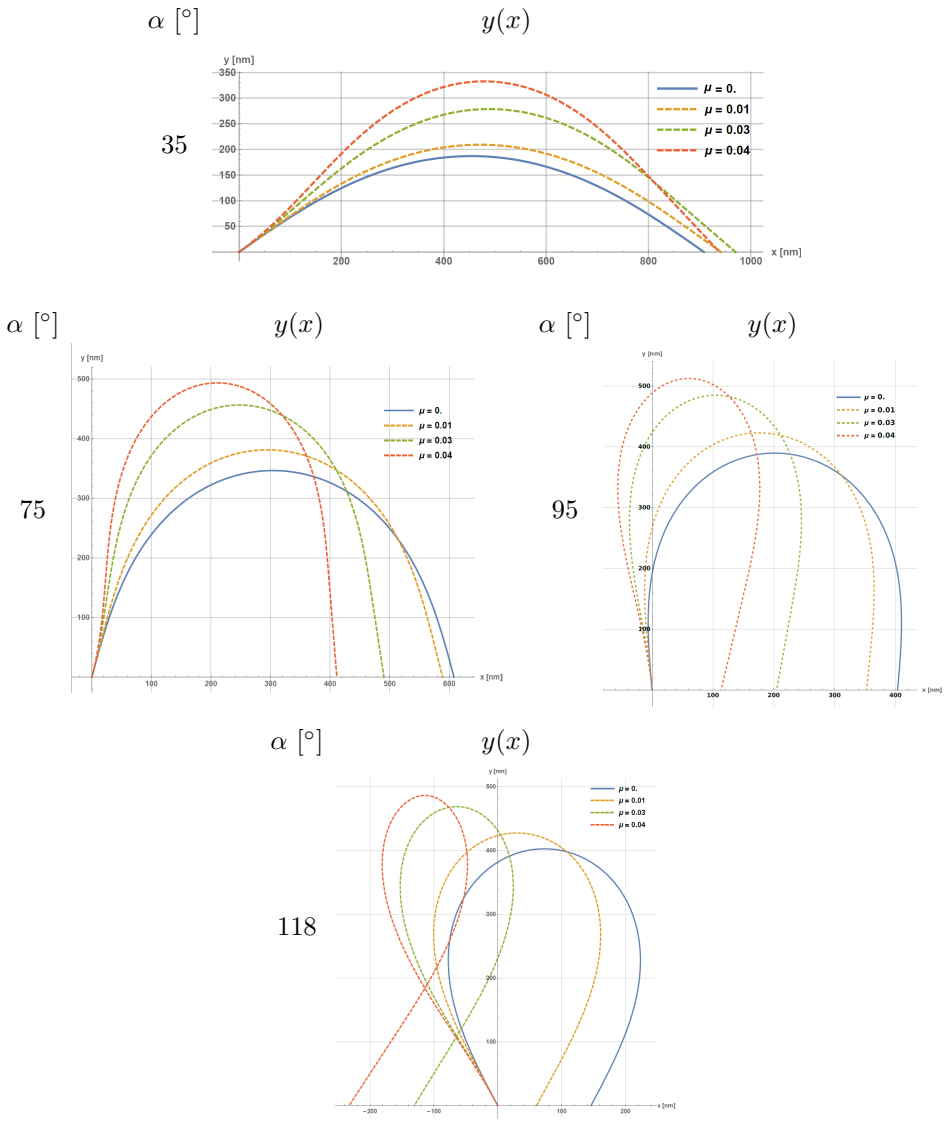

FIG. 4. Influence of the nonlocal theory on the shape of the elastica for given values of the initial angle α.

Further quantitative analysis of the maxima's position is presented in Table 3. It can be observed that the nonlocal theory implies an earlier onset of deformation, with a broadly similar overall form (though not identical, as evidenced by the left-side inflection of the rod). The maximum deflection does not occur at midspan (the problem becomes asymmetric, in contrast to the local formulation), and this tendency is most prominent for small initial angles. This is analyzed in detail in Table 3, where it can be seen that maximum is shifted from the midspan ($s = 500\,\mathrm{nm}$) to higher values of s. Moreover, we observe a small left-hand-side inflection, which is more pronounced for smaller values of the initial angle and for larger values of μ. For each initial angle, we extract also a critical value of the nonlocal parameter μ_{cr} (last row in Table 3), where the theory on our level of approximation breaks down. This is because the dominator in Eq. (2.26) approaches zero. The values of μ_{cr} decrease with increasing initial angle α.

TABLE 3. Quantitative analysis of the maxima position and the critical value of the nonlocal parameter μ_{cr}.

μ	$\alpha = 35^\circ$			$\alpha = 75^\circ$			$\alpha = 95^\circ$			$\alpha = 118^\circ$		
	$x_{\max}$	$y_{\max}$	$s_{\max}$	$x_{\max}$	$y_{\max}$	$s_{\max}$	$x_{\max}$	$y_{\max}$	$s_{\max}$	$x_{\max}$	$y_{\max}$	$s_{\max}$
0.00	454.3	186.9	500.0	304.0	346.3	500.0	201.8	389.503	500.0	73.04	402.4	500.0
0.01	471.0	209.1	525.0	294.6	381.1	523.5	176.5	422.697	522.0	30.3	427.3	518.8
0.03	488.9	278.7	575.3	247.6	456.3	564.8	104.3	484.667	559.0	−64.1	468.5	550.2
0.04	478.6	332.6	598.3	210.5	493.4	582.3	60.3	512.3	574.57	−114.2	486.1	563.7
μ_{cr}	0.0967			0.0809			0.06978			0.0551		

5. CONCLUSIONS

There are two main results that we obtained in this work. Firstly, we derived the nonlocal constitutive laws within Eringen's theory. These are equations for the derivative of the beam curvature, and their form is very similar to that of the classical Euler's elastica. This allows for a direct comparison of the two theories. One observes that the nonlocality appears in the denominator, which, in principle, may lead to instability. The second main result is that we have solved these equations numerically using the shooting method. The development and application of a novel numerical approach are a valuable outcome in themselves, as demonstrated by the widely cited work of CIVALEK *et al.* [80].

The computed results reveal a clear structural softening effect – the deformation becomes smoother, and the effective rigidity $EI_{\mathrm{eff}} = EI - \mu F \cos\theta(s)$ decreases, confirming the expected nonlocal influence predicted by Eringen's theory. We applied mixed boundary conditions at both ends, corresponding to

physical situations encountered in experiments for nanorods. Interestingly, while classical Euler's elastica shows symmetric bending, within the Eringen's theory there is clear asymmetry: the maximum curvature is shifted toward the left side of the beam. This effect can be considered a hallmark of the presence of nonlocal elasticity when the beams are measured experimentally.

Increasing the nonlocal parameter μ and the initial angle α brings the system closer to instability, which manifest as singular behavior in the curvature derivative. Further extension of the theory is required to mitigate this effect. If one considers that elastica theory is an effective continuum description that emerges upon averaging microscopic degrees of freedom, then one may suspect that including anharmonicity of the underlying lattice could prevent the occurrence of excessively large local curvature.

Eringen's theory remains a subject of ongoing debate, particularly with respect to its differential formulation. The specific values of the nonlocal parameter μ, which directly accounts for nonlocality in a given structure, are not yet well established. Since the problem has not been fully explored, a promising direction for the authors' future work is the implementation of constitutive boundary conditions, especially in studies that incorporate experimental data for specific materials. As described in Subsec. 2.1, constitutive boundary conditions are mathematically derived for a given propagator, and they allow to build a connection between differential and integral formulations of the theory. It is not clear what is their relationship to physically observed boundary conditions. In the future, one could add constitutive BCs into the shooting optimization procedure and/or investigate which propagators are imposed by a given physical setting. We believe these directions are fascinating future avenues for further research on nonlocality in nanostructures.

Appendix

Euler's formula

We consider a simply supported, elastic, inextensible circular rod of length l, subjected to a compressive load F applied at point B, as shown in Fig. 2. During compression, the rod changes its curvature and we can denote α as the initial angle at point A, u_1 is the displacement of the end of the rod at the right support from point B to C, and u_2 is the deflection at point X. The vectors $\mathbf{t}$ and $\mathbf{n}$ are the tangent and normal directions at point X, respectively.

The governing differential equation for the elastica can be expressed as [44]:

$$\theta(s)'' + \lambda^2 \sin\theta(s) = 0, \tag{A.1}$$

where θ is the angle of inclination of the tangent $\mathbf{t}$ to the elastica at point X, $\lambda^2 = \frac{F}{EI}$, F is the axially applied load, E is Young's modulus, I is the moment

of inertia, and $s \in [0, l]$ is the nondimensional arc-length parameter defined by its centerline.

From basic geometric considerations relating to the displacement vector (from point X_0 to X), we obtain the standard relation between curvature and the rotation angle of the tangent:

$$\varkappa = \frac{\mathrm{d}\theta}{\mathrm{d}s}. \tag{A.2}$$

The moment-curvature relationship can be expressed as [66]:

$$\varkappa = \frac{\mathrm{d}\theta}{\mathrm{d}s} = \frac{M}{EI}. \tag{A.3}$$

The boundary conditions for a simply supported beam are:

$$u_1(0) = 0, \tag{A.4}$$

$$u_2(0) = u_2(l) = 0, \tag{A.5}$$

$$\theta'(0) = \theta'(l) = 0. \tag{A.6}$$

These boundary conditions describe the theoretical framework of the classical Euler's buckling case, in which a slender elastic rod is subjected to axial compression between two hinged supports. In this formulation, the supports prevent transverse displacements while permitting free rotation, thereby providing a coherent mathematical representation of the problem. In our approach, we aim to obtain the elastica shape for a given initial angle and bifurcation mode m. In this case, the system of equations describing the elastica determines the corresponding coordinates x and y for each chosen point X along the rod axis.

Taking into account the boundary conditions (Eq. (A.4), Eq. (A.5), and Eq. (A.6)) and using elliptic integrals, we can solve the governing Eq. (2.1), obtaining the solution presented in [76]:

$$x = -s + \frac{2}{\lambda}\Big\{E\left[am\left(s\lambda + K(k), k\right), k\right] - E\left[am\left(K(k), k\right), k\right]\Big\}, \tag{A.7}$$

$$y = -\frac{2k}{\lambda} cn\left(s\lambda + K(k), k\right), \tag{A.8}$$

where $x, y \in \langle 0, l\rangle$ are the coordinates along the rod axes, $E(k)$ is the incomplete elliptic integral of the second kind with $E(x,k) = \int\limits_0^x \sqrt{1 - k\sin^2 t}\,\mathrm{d}t$, $k = \sin\frac{\alpha}{2}$, α is the initial angle with $\alpha = \theta(0)$ and $0 \leq \alpha \leq \pi$, and $K(k)$ is the complete elliptic integral of the first kind, defined as $K(k) = \int\limits_0^{\pi/2} \frac{\mathrm{d}\phi}{\sqrt{1-k^2\sin^2\phi}}$.

Using Eq. (A.7) and Eq. (A.8), the solution for a given initial angle α and mode m can be plotted. In Fig. A1, the elastica curves are shown for various values of the initial angles ($\alpha = 30°, 60°, 90°, 120°, 170°$, and $179°$) and for bifurcation modes $m = 1, 2, 3$, and 4. These results illustrate the post-critical behavior of the compressed rod. Figure A1 visualizes how the nonlinear post-buckling shapes evolve with different bifurcation modes m. Higher values of m lead to more complex deflection patterns and richer branches of solutions. The first mode ($m = 1$) is the most critical case, because it occurs at the lowest load and produces the largest midspan deflection. In the second mode ($m = 2$), the rod bends into two half-waves with a node at the midpoint. The midspan deflection is approximately half that of the first mode ($m = 1$) and occurs symmetrically upward and downward along the axis. It needs four times the critical load value of the first mode. In the third mode ($m = 3$), the rod exhibits three half-waves with two interior nodes. The midspan deflection is around three times smaller than that in the first mode $m = 1$, requiring nine times the critical load value. In the fourth mode ($m = 4$), the rod deforms into four half-waves with

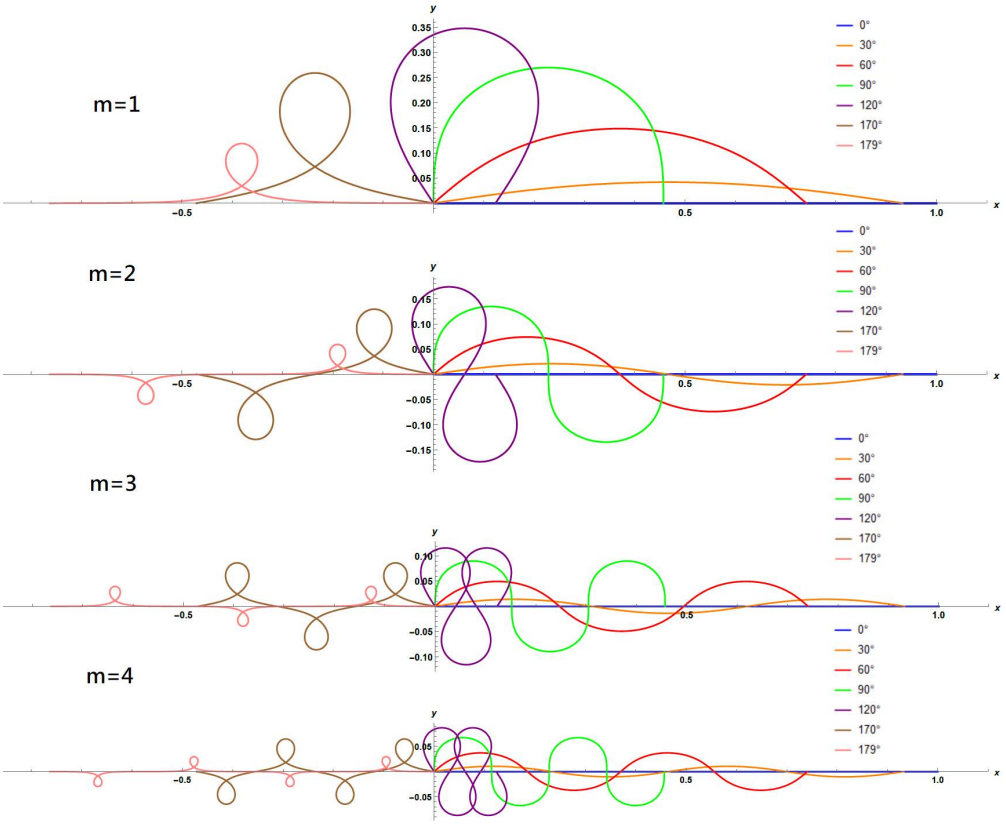

FIG. A1. Various shapes of elastica for given initial angles α and m-th modes of bifurcation.

three internal nodes. The maximum deflection is about one-quarter of that in the first mode ($m = 1$), while requiring a sixteen-fold increase in the critical load. The inherent symmetry of the problem is clearly reflected in these deformation patterns.

These particular initial angles (0°, 30°, 60°, 90°, 120°, 170°, 179°) were selected to illustrate the full spectrum of elastica behavior. For small angles (0° to 30°), the rod shows relatively gentle deflections with smooth, gradually increasing curvature. Medium angles (60° to 120°) highlight the stronger nonlinear character of the elastica, with curves bending more significantly and beginning to form loops, particularly in higher buckling cases. Very large angles (170° to 179°) correspond to extreme cases, where the rod shape approaches self-intersecting loops and folding. Because of its expected relevance for future experimental validation, the analysis concentrates mainly on the first buckling mode.

Fundings

This research did not receive any specific grant from funding agencies in the public, commercial, or not-for-profit sectors.

Conflict of interests

The authors declare that there are no known competing financial interests or personal relationships that could have influenced the work described in this paper.

Authors' contribution

Aleksandra Manecka-Padaż: supervision, conceptualization, methodology, validation, formal analysis, investigation, writing original draft. Ewa Eliza Rożko: methodology, data curation, validation, formal analysis, investigation, review and editing. Zdzisław Nowak: methodology, validation, formal analysis, investigation, review. Piotr Chudziński: methodology, validation, formal analysis, investigation, review. All authors reviewed and approved the final manuscript.

References

1. Zaccaria D., Bigoni D., Noselli G., Misseroni D., Structures buckling under tensile dead load, *Proceedings of the Royal Society A: Mathematical, Physical and Engineering Sciences*, **467**(2130): 1686–1700, 2011, https://doi.org/10.1098/rspa.2010.0505.
2. Bistafa S.R., Euler's variational approach to the elastica, *Euleriana*, **3**(2): 156–175, 2023, https://doi.org/10.56031/2693-9908.1055.

3. Matsutani S., Euler's elastica and beyond, *Journal of Geometry and Symmetry in Physics*, **17**: 45–86, 2010, https://projecteuclid.org/journalArticle/Download?urlId=10.7546%2Fjgsp-17-2010-45-86.

4. Kirchhoff G., On the equilibrium and motion of an elastic disc [in German: Über das Gleichgewicht und die Bewegung einer elastischen Scheibe], *Journal für die reine und angewandte Mathematik*, **40**: 5–88, 1850, http://eudml.org/doc/147439.

5. Born M., *Studies on the stability of the elastic line in the plane and in space under different limiting conditions* [in German: *Untersuchungen über die stabilität der elastischen Linie in Ebene und Raum: Unter verschiedenen Grenzbedingungen*], Vandenhoeck & Ruprecht, 1906.

6. Nishinari K., Nonlinear dynamics of solitary waves in an extensible rod, *Proceedings of the Royal Society A: Mathematical, Physical and Engineering Sciences*, **453**(1959): 817–833, 1997, https://doi.org/10.1098/rspa.1997.0045.

7. Chucheepsakul S., Monprapussorn T., Divergence instability of variable-arc-length elastica pipes transporting fluid, *Journal of Fluids and Structures*, **14**(6): 895–916, 2000, https://doi.org/10.1006/jfls.2000.0301.

8. Vassilev V.M., Djondjorov P.A., Mladenov I.M., Cylindrical equilibrium shapes of fluid membranes, *Journal of Physics A: Mathematical and Theoretical*, **41**: 435201, 2008, https://doi.org/10.1088/1751-8113/41/43/435201.

9. Kibach H., Ture Savadkoohi A., Lamarque C.-H., Free vibrations of an elastica around its post-buckled configurations, *International Journal of Non-Linear Mechanics*, **179**: 105250, 2025, https://doi.org/10.1016/j.ijnonlinmec.2025.105250.

10. Taloni A., Vilone D., Ruta G., General theory for plane extensible elastica with arbitrary undeformed shape, *International Journal of Engineering Science*, **193**: 103941, 2023, https://doi.org/10.1016/j.ijengsci.2023.103941.

11. Leanza S., Zhao R.R., Hutchinson J.W., The elastica with pre-stress due to natural curvature, *Journal of the Mechanics and Physics of Solids*, **190**: 105690, 2024, https://doi.org/10.1016/j.jmps.2024.105690.

12. Phungpaingam B., Chucheepsakul S., Postbuckling behavior of variable-arc-length elastica connected with a rotational spring joint including the effect of configurational force, *Meccanica*, **53**(10): 2619–2636, 2018, https://doi.org/10.1007/s11012-018-0847-x.

13. Lai B., Liew J.Y.R., Wang T., Buckling behaviour of high strength concrete encased steel composite columns, *Journal of Constructional Steel Research*, **154**: 27–42, 2019, https://doi.org/10.1016/j.jcsr.2018.11.023.

14. Wang Q., Zou H.L., Deng Z.C., Snap-through of an elastica under bilateral displacement control at a material point, *Acta Mechanica Sinica*, **36**(3): 727–734, 2020, https://doi.org/10.1007/s10409-020-00937-4.

15. Fraldi M., Palumbo S., Cutolo A., Carotenuto A.R., Bigoni D., Bimodal buckling governs human fingers' luxation, *Proceedings of the National Academy of Sciences of the United States of America*, **120**(44): e2311637120, 2023, https://doi.org/10.1073/pnas.2311637120.

16. Hathaipichitchai P., Klaycham K., Jiammeepreecha W., Athisakul C., Chucheepsakul S., Postbuckling behavior of variable-arc-length elastica pipe conveying fluid including effects of self-weight and pressure variation, *International Journal of Non-Linear Mechanics*, **164**: 104760, 2024, https://doi.org/10.1016/j.ijnonlinmec.2024.104760.

17. Curatolo M., Napoli G., Nardinocchi P., Turzi S., Swelling-driven soft elastic catapults, *International Journal of Non-Linear Mechanics,* **162**: 104727, 2024, https://doi.org/10.1016/j.ijnonlinmec.2024.104727.

18. Wang X., Qiu X., Elastica-plastica theory of Euler-Bernoulli beams subjected to concentrated loads, *Applied Mathematical Modelling*, **136**: 115623, 2024, https://doi.org/10.1016/j.apm.2024.07.030.

19. Matsutani S., Statistical mechanics of elastica for the shape of supercoiled DNA: Hyperelliptic elastica of genus three, *Physica A: Statistical Mechanics and its Applications*, **643**: 129799, 2024, https://doi.org/10.1016/j.physa.2024.129799.

20. Duan H.L., Wang J., Karihaloo B.L., Theory of elasticity at the nanoscale, [in:] *Advances in Applied Mechanics*, **42**: 1–68, 2009, https://doi.org/10.1016/S0065-2156(08)00001-X.

21. Wang G.-F., Feng X.-Q., Surface effects on buckling of nanowires under uniaxial compression, *Applied Physics Letters*, **94**(14): 141913, 2009, https://doi.org/10.1063/1.3117505.

22. Moradi M., Fereidon A.H., Sadeghzadeh S., Dynamic modeling for nanomanipulation of polystyrene nanorod by atomic force microscope, *Scientia Iranica*, **18**(3): 808–815, 2011, https://doi.org/10.1016/j.scient.2011.06.003.

23. Liu J.L., Mei Y., Xia R., Zhu W.L., Large displacement of a static bending nanowire with surface effects, *Physica E: Low-Dimensional Systems and Nanostructures*, **44**(10): 2050–2055, 2012, https://doi.org/10.1016/j.physe.2012.06.009.

24. Thongyothee C., Chucheepsakul S., Postbuckling of unknown-length nanobeam considering the effects of nonlocal elasticity and surface stress, *International Journal of Applied Mechanics*, **7**(3): 1550042, 2015, https://doi.org/10.1142/S1758825115500428.

25. Challamel N., Kocsis A., Wang C.M., Discrete and nonlocal elastica, *International Journal of Non-Linear Mechanics*, **77**: 128–140, 2015, https://doi.org/10.1016/j.ijnonlinmec.2015.06.012.

26. Lembo M., Exact solutions for postbuckling deformations of nanorods, *Acta Mechanica*, **228**(6): 2283–2298, 2017, https://doi.org/10.1007/s00707-017-1834-3.

27. Tang Y., Qing H., Bending, buckling and free vibration of Timoshenko beam-based plane frame via FEM with nonlocal integral model, *Journal of Mechanics of Materials and Structures*, **18**(3): 355–374, 2023, https://doi.org/10.2140/jomms.2023.18.355.

28. Hussain M., Naeem M.N., Vibration characteristics of single-walled carbon nanotubes based on nonlocal elasticity theory using wave propagation approach (WPA) including chirality, [in:] *Perspective of Carbon Nanotubes*, El-Din Saleh H., El-Sheikh S.M.M. [Eds], 2019, https://doi.org/10.5772/intechopen.85948.

29. Berecki D., Glavardanov V.B., Grahovac N.M., Zigic M.M., Bifurcation analysis of a nanotube through which passes a nanostring, *Acta Mechanica*, **235**: 6867–6888, 2024, https://doi.org/10.1007/s00707-024-04076-w.

30. Darban H., Fabbrocino F., Feo L., Luciano R., Size-dependent buckling analysis of nanobeams resting on two-parameter elastic foundation through stress-driven nonlocal elasticity model, *Mechanics of Advanced Materials and Structures*, **28**(23): 2408–2416, 2021, https://doi.org/10.1080/15376494.2020.1739357.

31. Darban H., Luciano R., Darban R., Buckling of cracked micro- and nanocantilevers, *Acta Mechanica*, **234**(2): 693–704, 2023, https://doi.org/10.1007/s00707-022-03417-x.

32. Darban H., Elastostatics of nonuniform miniaturized beams: Explicit solutions through a nonlocal transfer matrix formulation, *International Journal of Engineering Science*, **198**: 104054, 2024, https://doi.org/10.1016/j.ijengsci.2024.104054.

33. Reddy J.N., Nonlocal theories for bending, buckling and vibration of beams, *International Journal of Engineering Science*, **45**(2–8): 288–307, 2007, https://doi.org/10.1016/j.ijengsci.2007.04.004.

34. Phadikar J.K., Pradhan S.C., Variational formulation and finite element analysis for nonlocal elastic nanobeams and nanoplate, *Computational Materials Science*, **49**(3): 492–499, 2010, https://doi.org/10.1016/j.commatsci.2010.05.040.

35. Aydogdu M., A general nonlocal beam theory: Its application to nanobeam bending, buckling and vibration, *Physica E: Low-dimensional Systems and Nanostructures*, **41**(9): 1651–1655, 2009, https://doi.org/10.1016/j.physe.2009.05.014.

36. Challamel N., Wang C.M., Elisahakoff I., Discrete systems behave as nonlocal structural elements: Bending, buckling and vibration analysis, *European Journal of Mechanics – A/Solids*, **44**: 125–135, 2014, https://doi.org/10.1016/j.euromechsol.2013.10.007.

37. Shaat M., Abdelkefi A., New insights on the applicability of Eringen's nonlocal theory, *International Journal of Mechanical Sciences*, **121**: 67–75, 2017, https://doi.org/10.1016/j.ijmecsci.2016.12.013.

38. Surmont F., Coache D., Geometrically exact static 3D Cosserat rods problem solved using a shooting method, *International Journal of Non-Linear Mechanics*, **119**: 103330, 2020, https://doi.org/10.1016/j.ijnonlinmec.2019.103330.

39. Darban H., Luciano R., Basista M., Free transverse vibrations of nanobeams with multiple cracks, *International Journal of Engineering Science*, **177**: 103703, 2022, https://doi.org/10.1016/j.ijengsci.2022.103703.

40. Singh J., Shooting method for solving two-point boundary value problems in ODEs numerically, [in:] *Artificial Intelligence Technology in Healthcare*, CRC Press, 2024, https://doi.org/10.1201/9781003377818-7.

41. Zorić A., Trajković-Milenković M., Zlatkov D., Vacev T., Semi-analytical solution for elastoplastic deflection of non-prismatic cantilever beams with circular cross-section, *Applied Sciences*, **12**(11): 5439, 2022, https://doi.org/10.3390/app12115439.

42. Eringen A.C., Linear theory of nonlocal elasticity and dispersion of plane waves, *International Journal of Engineering Science*, **10**(5): 425–435, 1972, https://doi.org/10.1016/0020-7225(72)90050-X.

43. Eringen A.C., Edelen D.G.B., On nonlocal elasticity, *International Journal of Engineering Science*, **10**(3): 233–248, 1972, https://doi.org/10.1016/0020-7225(72)90039-0.

44. Eringen A.C., On differential equations of nonlocal elasticity and solutions of screw dislocation and surface waves, *Journal of Applied Physics*, **54**(9): 4703–4710, 1983, https://doi.org/10.1063/1.332803.

45. Romano G., Barretta R., Nonlocal elasticity in nanobeams: The stress-driven integral model, *International Journal of Engineering Science*, **115**: 14–27, 2017, https://doi.org/10.1016/j.ijengsci.2017.03.002.

46. Nobili A., Pramanik D., A well-posed theory of linear nonlocal elasticity, *International Journal of Engineering Science*, **215**: 104314, 2025, https://doi.org/10.1016/j.ijengsci.2025.104314.

47. Barretta R., Feo L., Luciano R., Marotti de Sciarra F., Application of an enhanced version of the Eringen differential model to nanotechnology, *Composites Part B: Engineering*, **96**: 274–280, 2016, https://doi.org/10.1016/j.compositesb.2016.04.023.

48. Fernández-Sáez J., Zaera R., Loya J.A., Reddy J.N., Bending of Euler–Bernoulli beams using Eringen's integral formulation: A paradox resolved, *International Journal of Engineering Science*, **99**: 107–116, 2016, https://doi.org/10.1016/j.ijengsci.2015.10.013.

49. Ceballes S., Larkin K., Rojas E., Ghaffari S.S., Abdelkefi A., Nonlocal elasticity and boundary condition paradoxes: A review, *Journal of Nanoparticle Research*, **23**: 66, 2021, https://doi.org/10.1007/s11051-020-05107-y.

50. Kaplunov J., Prikazchikov D.A., Prikazchikova L., On integral and differential formulations in nonlocal elasticity, *European Journal of Mechanics – A/Solids*, **100**: 104497, 2023, https://doi.org/10.1016/j.euromechsol.2021.104497.

51. Pham C.V., Vu T.N.A., On the well-posedness of Eringen's non-local elasticity for harmonic plane wave problems, *Proceedings of the Royal Society A: Mathematical, Physical and Engineering Sciences*, **480**(2293): 20230814, 2024, https://doi.org/10.1098/rspa.2023.0814.

52. Barretta R., Luciano R., Marotti de Sciarra F.M., Vaccaro M.S., Modelling issues and advances in nonlocal beams mechanics, *International Journal of Engineering Science*, **198**: 104042, https://doi.org/10.1016/j.ijengsci.2024.104042.

53. Song Z.W., Lai S.K., Lim C.W., Li C., Theoretical examination for the consistency of Eringen's nonlocal theories in nanomaterial modeling, *International Journal of Applied Mechanics*, **17**(06): 2550044, 2025, https://doi.org/10.1142/S1758825125500449.

54. Pramanik D., Nobili A., A well-posed non-local theory in 1D linear elastodynamics, *International Journal of Solids and Structures*, **320**: 113511, 2025, https://doi.org/10.1016/j.ijsolstr.2025.113511.

55. Pisano A.A., Fuschi P., Polizzotto C., Euler–Bernoulli elastic beam models of Eringen's differential nonlocal type revisited within a C^0 – Continuous displacement framework, *Meccanica*, **56**: 2323–2337, 2021, https://doi.org/10.1007/s11012-021-01361-z.

56. Song Z.W., Lai S.K., Lim C.W., A new insight into the paradoxical integral and differential constitutive relations of Eringen nonlocal theory, *Journal of Engineering Mechanics*, **151**(2): 04024112, 2025, https://doi.org/10.1061/JENMDT.EMENG-8021.

57. Song Z.W., Lai S.K., Lim C.W., On the truth of integral and differential constitutive forms in strain-driven nonlocal theories with bi-Helmholtz kernels for nanobeam analysis, *Thin-Walled Structures*, **214**: 113338, 2025, https://doi.org/10.1016/j.tws.2025.113338.

58. Song Z.W., Lai S.K., Lim C.W., On the nature of constitutive boundary and interface conditions in stress-driven nonlocal integral model for nanobeams, *Applied Mathematical Modelling*, **144**: 115949, 2025, https://doi.org/10.1016/j.apm.2025.115949.

59. Karličić D., Murmu T., Adhikari S., McCarthy M., *Nonlocal Structural Mechanics*, John Wiley & Sons, 2016, https://doi.org/10.1002/9781118572030.

60. Lu P., Lee H.P., Lu C., Zhang P.Q., Dynamic properties of flexural beams using a nonlocal elasticity model, *Journal of Applied Physics*, **99**(7): 073510, 2006, https://doi.org/10.1063/1.2189213.

61. Timesli A., An efficient approach for prediction of the nonlocal critical buckling load of double-walled carbon nanotubes using the nonlocal Donnell shell theory, *SN Applied Sciences*, **2**: 407, 2020, https://doi.org/10.1007/s42452-020-2182-9.

62. Wang C.M., Zhang Y.Y., Ramesh S.S., Kitipornchai S., Buckling analysis of micro- and nano-rods/tubes based on nonlocal Timoshenko beam theory, *Journal of Applied Physics*, **39**(17): 3904–3909, 2006, https://doi.org/10.1088/0022-3727/39/17/029.

63. Reddy J.N., Pang S.D., Nonlocal continuum theories of beams for the analysis of carbon nanotubes, *Journal of Applied Physics*, **103**(2): 023511, 2008, https://doi.org/10.1063/1.2833431.

64. Wang L., Hu H., Flexural wave propagation in single-walled carbon nanotubes, *Physical Review B – Condensed Matter and Materials Physics*, **71**(19): 195412, 2005, https://doi.org/10.1103/PhysRevB.71.195412.

65. Akpinar M., Uzun B., Yayli M.Ö., Dynamic response of axially loaded carbon nanotubes considering armchair, chiral, and zigzag configurations, *Mechanics Based Design of Structures and Machines*, **54**(1): 2553325, 2025, https://doi.org/10.1080/15397734.2025.2553325.

66. Natsuki J., Lei X.-W., Wu S., Natsuki T., Modeling and vibration analysis of carbon nanotubes as nanomechanical resonators for force sensing, *Micromachines*, **15**(9): 1134, 2024, https://doi.org/10.3390/mi15091134.

67. Uzun B., Yayli M.Ö., Civalek Ö., Elastic medium and torsional spring effects on the nonlocal dynamic of functionally graded porous nanotubes, *Archive of Applied Mechanics*, **94**: 1291–1311, 2024, https://doi.org/10.1007/s00419-024-02576-8.

68. Ebrahimi R., Chaotic vibrations of carbon nanotubes subjected to a traversing force considering nonlocal elasticity theory, *Proceedings of the Institution of Mechanical Engineers, Part N: Journal of Nanomaterials, Nanoengineering and Nanosystems*, **236**(1–2): 31–40, 2022, https://doi.org/10.1177/23977914211063309.

69. Murmu T., Pradhan S.C., Small-scale effect on the vibration of nonuniform nanocantilever based on nonlocal elasticity theory, *Physica E: Low-dimensional Systems and Nanostructures*, **41**: 1451–1456, 2009, https://doi.org/10.1016/j.physe.2009.04.015.

70. Wang C.M., Zhang Z., Challamel N., Duan W.H., Calibration of Eringen's small length scale coefficient for initially stressed vibrating nonlocal Euler beams based on microstructured beam model, *Journal of Physics D: Applied Physics*, **46**(34): 345501, 2013, https://doi.org/10.1088/0022-3727/46/34/345501.

71. Khaniki H.B., Hosseini-Hashemi S., Buckling analysis of tapered nanobeams using nonlocal strain gradient theory and a generalized differential quadrature method, *Materials Research Express*, **4**(6): 065003, 2017, https://doi.org/10.1088/2053-1591/aa7111.

72. Thongyothee Ch., Chucheepsakul S., Postbuckling behaviors of nanorods including the effects of nonlocal elasticity theory and surface stress, *Journal of Applied Physics*, **114**(24): 243507, 2013, https://doi.org/10.1063/1.4829896.

73. Lu P., Lee H.P., Lu C., Zhang P.Q., Dynamic properties of flexural beams using a nonlocal elasticity model, *Journal of Applied Physics*, **99**(7): 073510, 2017, https://doi.org/10.1063/1.2189213.

74. De Rosa M.A., Lippiello M., Babilio E., Ceraldi C., Nonlocal vibration analysis of a nonuniform carbon nanotube with elastic constraints and an attached mass, *Materials*, **14**(13): 3445, 2021, https://doi.org/10.3390/ma14133445.

75. Euler L., On stability of column [in Latin: De motu columnarum erectarum], [in:] *Novi Commentarii academiae scientiarum Petropolitanae*, **10**: 99–140, 1757 (published 1759).

76. Bigoni D., *Nonlinear Solid Mechanics: Bifurcation Theory and Material Instability*, Cambridge University Press, 2012.

77. Manecka-Padaż A., Jenczyk P., Pęcherski R.B., Nykiel A., Experimental investigation of Euler's elastica: In-situ SEM nanowire post-buckling, *Bulletin of the Polish Academy of Sciences, Technical Sciences*, **70**(6): e143648, 2022, https://doi.org/10.24425/bpasts.2022.143648.

78. Dormand J.R., Prince P.J., A family of embedded Runge-Kutta formulae, *Journal of Computational and Applied Mathematics*, **6**(1): 19–26, 1980, https://doi.org/10.1016/0771-050X(80)90013-3.

79. Calvo M., Montijano J.I., Randez L., A fifth-order interpolant for the Dormand and Prince Runge-Kutta method, *Journal of Computational and Applied Mathematics*, **29**(1): 91–100, 1990, https://doi.org/10.1016/0377-0427(90)90198-9.

80. Civalek Ö., Demir Ç., Bending analysis of microtubules using nonlocal Euler–Bernoulli beam theory, *Applied Mathematical Modelling*, **35**(5): 2053–2067, 2011, https://doi.org/10.1016/j.apm.2010.11.004.

Received October 31, 2025; revised December 1, 2025; accepted December 6, 2025; available online December 12, 2025; version of record May 15, 2026; published issue June 24, 2026.